Third-generation megahertz-rate pulse burst laser system

Brian S. Thurow,[1,*] Aman Satija,[1,2] and Kyle Lynch[1]

[1]Department of Aerospace Engineering, Auburn University, 211 Davis Hall, Auburn, Alabama 36849, USA

[2]Purdue University, West Lafayette, Indiana 47907, USA

*Corresponding author: thurow@auburn.edu

Received 20 May 2008; revised 9 September 2008; accepted 12 September 2008; posted 17 September 2008 (Doc. ID 96418); published 2 April 2009

The design and performance of a third-generation megahertz-rate pulse burst laser system is described. The third-generation system incorporates two distinct design changes that distinguish it from earlier-generation systems. The first is that pulse slicing is now achieved by using an economical acousto-optic modulator (AOM), and the second is the use of a variable pulse duration flashlamp driver that provides relatively uniform gain over a $\sim 700\,\mu$s window. The use of an AOM for pulse slicing permits flexible operation such as pulse-on-demand operation with variable pulse durations ranging from 10 ns to DC. The laser described here is capable of producing a burst of laser pulses at repetition rates as high as 50 MHz and peak powers of 10 kW. Second-harmonic conversion efficiency using a type II KTP crystal is also demonstrated. © 2009 Optical Society of America

OCIS codes: 140.0140, 140.3530, 140.3538, 280.2490.

1. Introduction

Utilization of pulsed Nd:YAG lasers for aerodynamic measurements has steadily increased over the past few decades as these lasers have become commercially available in a relatively robust, compact, and affordable package [1]. The high energy (of the order of a millijoule per pulse and higher) and short pulse duration (on the order of 10 ns) provided by these lasers allow nearly instantaneous flow measurements with relatively high signal-to-noise ratios. Numerous techniques have been developed based on these capabilities for measurements in turbulent and reacting flows. These include, but are not limited to, planar laser Mie scattering, particle image velocimetry, planar laser-induced fluorescence, planar Doppler velocimetry, and coherent anti-Stokes Raman scattering and can be found in numerous research laboratories around the world. Although the current work is motivated by aerospace applications, pulsed Nd:YAG lasers are utilized throughout the scientific community and industry for a multitude of purposes.

A significant shortcoming of currently available pulsed Nd:YAG laser systems is the maximum repetition rate that these systems can achieve. The repetition rate is primarily limited by the thermal loading of the pump source on the Nd:YAG gain medium, which is typically cooled by circulating water through the pump chamber. For flashlamp-pumped systems, which are relatively inefficient owing to the broadband output of the flashlamp, repetition rates of the order of 10–100 Hz are common. More recently developed diode-pumped systems, which are less thermally demanding owing to the relatively narrow bandwidth of laser diodes, allow continuous pumping of the gain medium, enabling repetition rates on the order of 10 kHz with pulse energies on the order of 1 mJ/pulse. Higher repetition rates, however, are limited by the expense and limited peak power of currently available diode pump lasers.

High-speed turbulent flow fields, particularly those associated with supersonic flows, however, are commonly characterized by turbulent time scales of the order of microseconds and require even

0003-6935/09/112086-08$15.00/0

higher-repetition-rate laser sources (megahertz order) to probe the dynamic features of these flow fields. In addition, the development and adoption of other novel measurement techniques is somewhat restrained by the repetition rate of commercially available laser systems. For example, we have recently developed a high-speed 3D flow visualization system based on the scanning and imaging of a high-repetition-rate laser sheet through the flow field [2].

This paper describes the design of a third-generation pulse burst laser system capable of repetition rates in excess of 1 MHz and pulse energies on the order of 1 mJ/pulse. The overall design is based on laser systems previously developed and referred to here as first-generation [3,4] and second-generation systems [5,6]. Similar systems based on these earlier designs have also been built elsewhere [7,8]. Before discussing the current system, a brief synopsis of the design of these earlier systems is offered.

The basic scheme employed has been that of a master oscillator power amplifier, where a burst of pulses is formed initially at low power and subsequently amplified through a chain of flashlamp-pumped power amplifiers. The master oscillator consists of a low-power (20–100 mW) continuous wave (cw) Nd:YAG laser operating at 1.064 μm. The cw laser beam is then preamplified and double-passed through a pair of Pockels cells, which are used to slice the cw laser beam into a burst of low-energy pulses. Two Pockels cells, each requiring a high-voltage excitation source, are required in order to achieve the fast rise and fall time necessary to form pulses with order 10 ns duration. Following formation of the low-energy burst of pulses, the pulses are passed through a series of flashlamp-pumped Nd:YAG rod power amplifiers with an overall system gain of 10^6–10^8, depending on the number of amplifiers in the chain. Electrical current to the flashlamps is provided by using conventional pulsed flashlamp controllers, resulting in a temporal gain profile that is approximately Gaussian in shape and $\sim$200 μs in length. This mode of operation avoids the thermal management issues discussed above by keeping the overall duty cycle of the system low. A drawback to this arrangement is that the gain is available only over a short period of time and is not constant across a burst of pulses, as the gain varies with the current provided to the flashlamps. Still, pulse energies over 100 mJ/pulse in bursts consisting of 10 s of pulses have been achieved, and the utility of these systems for aerodynamic measurements has been well demonstrated [2–8].

This paper details the design of a third-generation pulse burst laser system. The design of the current system is conceptually the same as the systems described above; however, it incorporates two distinct design changes that are the focus of this paper. The first is the use of an acousto-optic modulator (AOM) for pulse slicing as opposed to the pair of more expensive Pockels cells used in previous work. The second is the use of a variable-pulse-width flashlamp controller that provides relatively uniform gain over a 700 μs window. Overall, these changes make the laser more economical to build and provide for more flexible operation, allowing for it to be used in a greater range of applications.

2. Third-Generation Pulse Burst Laser System Design

The design of the pulse burst laser system can be divided into two fundamental parts: the pulse slicer and the power amplifier chain. The function of the pulse slicer is to slice the output of a cw laser into a burst of low-energy (nanojoule order) short-duration pulses. These pulses are then amplified by several orders of magnitude in the power amplifier chain. A description of these components is given below.

A. Acousto-optic Modulator Pulse Slicer

A burst of low-energy laser pulses can be formed by slicing the output of a cw laser beam. In previous work, this slicing was achieved by using a pair of Pockels cells, which can form pulses less than 10 ns in duration at repetition rates as high as 1 MHz. Although effective, this method of slicing is not used here for multiple reasons. First, a pair of high-speed Pockels cells and the associated high-speed, high-voltage electronics are not readily available as an off-the-shelf system and would have to be specially designed and built. Related to this, the original manufacturer of the pulse slicers used in previous systems is no longer in business, and there would be some additional risk associated with trying a new design. Thus this approach turned out to be too costly to pursue. In addition, the high-voltage electronics present some safety and reliability concerns and would not be easily replaced or repaired in the event of failure. An alternative, and much more economical (by an order of magnitude), method of creating a burst of pulses from a cw laser beam is through the use of an AOM. AOMs have been in use for several decades, and their principles of operation are well known (see, for example, Korpel [9]). A brief review of the most pertinent characteristics of AOMs with respect to the current application is provided below.

1. *Theory of Operation*

AOMs, also commonly referred to as Bragg cells, operate on the principles of the acousto-optic (AO) effect, where an acoustic wave, introduced via a piezoelectric transducer, travels through a crystal or liquid, causing a small variation in the index of refraction. This variation appears to an optical beam passing through the medium as a sinusoidal grating with wavelength equal to the acoustic wavelength. Thus, incident light will be diffracted in the presence of the acoustic wave. Most AO devices operate in the Bragg regime, where most of the incident light can be diffracted into the first-order beam fairly efficiently.

For the current application, we are interested in slicing pulses of light from a cw laser beam. This can be done by rapidly turning the deflection on or off via control of the acoustic waves inside the AO crystal. In this case, the deflected laser beam constitutes the desired burst of pulses with the beam being deflected only when a positive voltage is applied to the AOM driver. As we are interested in the formation of short-duration (10s of nanosecond) pulses, the most important properties are the rise–fall time, diffraction efficiency, and contrast ratio of the AOM and driver.

The rise time, t_r, of the deflected pulse is limited primarily by the time it takes for the acoustic wave to travel across the aperture of the beam. With acoustic velocities on the order of several thousand meters per second, rise times of a few nanoseconds can be achieved by tightly focusing the beam inside the crystal. Additional factors that can affect the rise time of the laser pulses are the intensity profile of the incident beam (e.g., TEM_{00}) and the speed of the AOM RF driver and pulse generator. In this work, a rise time of ~10 ns has been achieved, which is slower than the 3–4 ns rise times achieved with Pockels cells, but still fast enough for the intended applications of the laser.

The diffraction efficiency of an AOM depends on the acoustic power, material properties, geometry, and wavelength of light. In general, the intensity of the diffracted beam can range from a few percent to >90% of the incident beam. An overall efficiency of ~60% is realized in the current work, which is less than the >90% efficiency achieved with Pockels cells. Unlike some other AOM applications, such as Q switches, the pulse slicer is not an intracavity device. Thus, the relatively poor efficiency of the AOM does not result in an exponential decrease in power as it would if it were placed within an oscillator. Rather, the reduction can be compensated for by increasing the duration of the pulse or building more gain into the amplifier system. It is important to keep in mind that in systems with large gain, doubling the pulse energy at this early stage does not necessarily correspond to a doubling of pulse energy after amplification.

Last, the contrast ratio of the AOM is another important parameter. Also referred to as the extinction ratio, it is the ratio of the light intensity when the AOM is turned on to when it is turned nominally off. The contrast ratio is important because any light passing through the amplifiers when the slicer is off (i.e., when no pulses are desired) will be amplified and reduce the overall efficiency of the system, particularly at later stages of amplification where pulses are no longer in the small-signal gain regime. Because the slicer is off much longer than it is on (20 ns versus 1 μs), this can cause a significant loss of the energy stored in the amplifiers and limit the energy available for amplification of the pulses. The intensity of light when the AOM is turned off is primarily caused by impurities in the crystal, scattered or diffracted light from various optics in the system, and leakage RF power from the modulator driver. Typical AOMs have a contrast ratio ranging from 500:1 to 1000:1, which is similar to that achieved by using Pockels cells. The contrast ratio can be increased by spatially filtering the diffracted laser beam, which helps minimize the contribution of scattered or diffracted light, and by using a modulator driver with a high extinction ratio.

2. *Measured Pulse Characteristics*

Figure 1 contains a schematic of the AOM pulse slicer arrangement. The overall footprint is ~40 × 15 cm. The master oscillator is a 100 mW single-longitudinal-mode Nd:YAG cw laser (CrystaLaser, Reno, Nevada) with output at 1.064 μm. The narrow linewidth of the seed laser is not necessary for the formation of pulse bursts but is desirable for efficient harmonic conversion and potential use in spectroscopic-based measurements. The 0.4 mm diameter beam of the cw laser is first passed through a Faraday isolator and then expanded by a −15 mm focal length plano–concave lens and focused into the AOM with a +50 mm plano–convex lens to produce a spot size of approximately 40 μm. The AOM (Brimrose GPM-400-100-1060) is mounted on a stage that provides both rotation and translation so that the focused spot can be positioned within the active portion of the AO crystal with an incident angle equal to the Bragg angle. The AO crystal is gallium phosphide, which has an acoustic velocity of 6300 m/s. This gives a calculated minimum rise time of ~6 ns according to $t_r = D/V_a$, where V_a is the acoustic velocity and D is the diameter of the focused beam within the AO medium. The acoustic wave within the crystal is powered by a 1.5 W, 400 MHz RF Source (Brimrose FFA-400-B2-F1.5-X). It has a specified rise time of 3.5 ns and an extinction ratio of >50 dB. The modulation is controlled via an externally applied TTL (transistor–transistor logic) signal by using a National Instruments Counter/Timer (NI-6602) card and has a digital modulation bandwidth of DC–100 MHz. Thus, bursts with repetition rates as high as 100 MHz are possible. The AOM is able to direct approximately 55% of the incident power into the first order ($\Delta\theta = 67$ mrad) with an aperture used to remove the rest of the modes. The burst of pulses is then collimated and directed to the amplifier system.

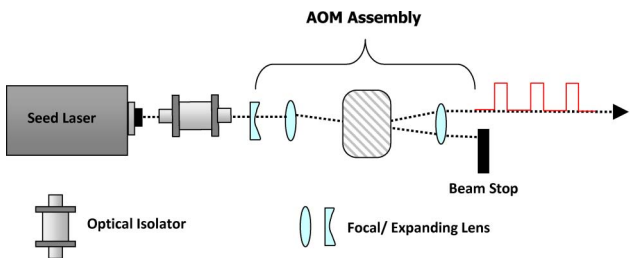

Fig. 1. (Color online) Schematic of AOM pulse slicer.

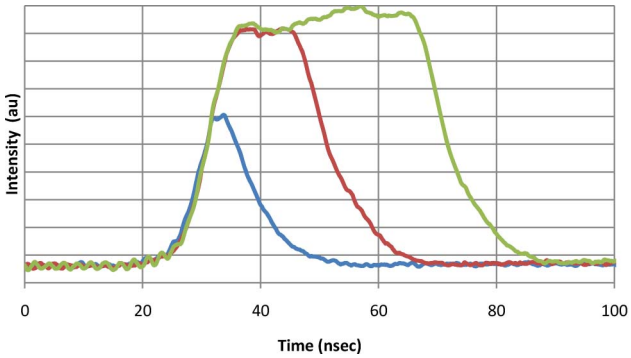

Fig. 2. (Color online) Oscilloscope trace of 10, 20, and 40 ns pulses formed using AOM pulse slicer.

Figure 2 shows an oscilloscope trace (500 MHz, Tektronix TDS5054B) for 10, 20, and 40 ns duration pulses (FWHM). The waveforms were acquired with a high-speed photodetector (Thorlabs DET210) with a rise time of 1 ns. There is slight delay of approximately 200 ns between the command input (not shown) and the pulse formation, which is due mainly to the travel time of the acoustic wave in the AOM from the piezoelectric oscillator to the location of the beam in the crystal. The measured rise–fall time of the pulses is approximately 10 ns. This agrees relatively well with an expected rise time of ~8 ns when the rise time of the pulse generator (3 ns), modulator driver (3.5 ns), and acoustic velocity (~6 ns, according to $t_r = D/V_a$) are taken into account. An inherit strength of the AOM is the ability to form pulses on demand, with the only limitation being the 10 ns rise time of the pulse. This is apparent when considering the 10 ns duration pulse, which has lower amplitude than the 20 ns pulse. Longer pulses have a shape similar to the 40 ns pulse, with the power being approximately constant over time. The peak power at this point is estimated to be ~60 mW, which is the power measured when the beam is continuously deflected by the AOM.

The contrast ratio of the pulses was determined by measuring the power with the AOM turned off and the cw laser turned on. A Coherent LM-2 VIS power detector with a sensitivity as low as 10 nW was used to detect the small amount of laser light that leaks through when the AOM is off. With the powermeter positioned immediately after the aperture, approximately 60–90 μW of laser light was detected even with the AOM turned off. 60 mW was measured with the AOM on. This yields a contrast ratio of ~800± 200. This is similar in magnitude to what would be expected with a pair of Pockels cells. Spatially filtering the signal can increase the contrast ratio by filtering out the portion of light that is due to off-axis scattering caused by impurities in the crystal, diffraction from lenses and other optics, or even dust in the air. With spatial filtering, the contrast ratio was found to increase to $\sim 15,000 \pm 2000$.

The drawback to spatial filtering is that it reduces the signal slightly (to ~50 mW), can be difficult to align, and is prone to drift out of alignment over time. It was thought that the long path length (~2.5 m) and finite aperture of the amplifier chain should have a similar effect as the spatial filter. This was examined by measuring the contrast ratio of the pulses after passage through the amplifier chain, but with the amplifiers turned off. In this case, the contrast ratio was measured to be $\sim 20,000:1$ without a spatial filter. Thus the spatial filter is not currently used in the system. The contrast ratio reported here is significantly higher than would be expected when a pair of Pockels cells is used for slicing. One reason for this is that pulses deflected by the AOM follow a different optical path than the incident cw laser beam, thus making it easier to separate the pulses from the original cw beam. While not necessary in the current system, it should be noted that the contrast ratio can be further increased by the addition of a second AOM or the addition of a phase conjugate mirror. [4]

B. Power Amplifier Chain

Following formation of the burst of low-energy pulses, the pulses must be amplified by a factor of 10^5 or greater to be generally useful for fluid dynamic measurements. This amplification is provided by a chain of three flashlamp-pumped double-pass Nd:YAG rod amplifiers. A schematic of the power amplifier chain is shown in Fig. 3. The input beam (pulses) from the pulse slicer is enlarged to 4 mm in diameter with a telescope prior to entering the power amplifier chain. The beam then passes through a polarizer and into the first amplifier, which has a diameter of 4 mm and length of 100 mm. The amplified beam (single pass) then passes through a $\lambda/4$ wave plate, reflects from a 0° mirror, travels back through the wave plate (for a net retardation of $\lambda/2$) and back through the amplifier (second pass) and then is reflected by the polarizer to the next amplifier. This process is repeated for the second and third amplifiers, which have diameters of 5 and 6.3 mm, respectively. The pulse energy supplied to the flashlamps is approximately 20, 30, and 40 J over a 1 ms pulse duration, respectively. Optical isolators are contained between each amplification stage in an effort to prevent parasitic lasing and amplified spontaneous emission (ASE), problems that were significant in the development of earlier systems. A telescope is placed between the first and the second stage to increase the beam size to match the aperture of the Nd:YAG rods and to counteract the thermal lensing associated with the amplifiers. Thermal lensing imposes a slight focusing effect on the beam (estimated focal length around 2 m). While this made the system slightly more difficult to align, we did not detect any significant changes to the beam mode or quality.

The most significant change to the amplifier chain in the current work is the temporal gain curve of the amplifier chain. In previous designs, the power supply for the amplifiers was similar in design to those used in commercial Nd:YAG lasers designed for single-pulse operation. As such, these systems were characterized by a Gaussian-shaped gain curve with

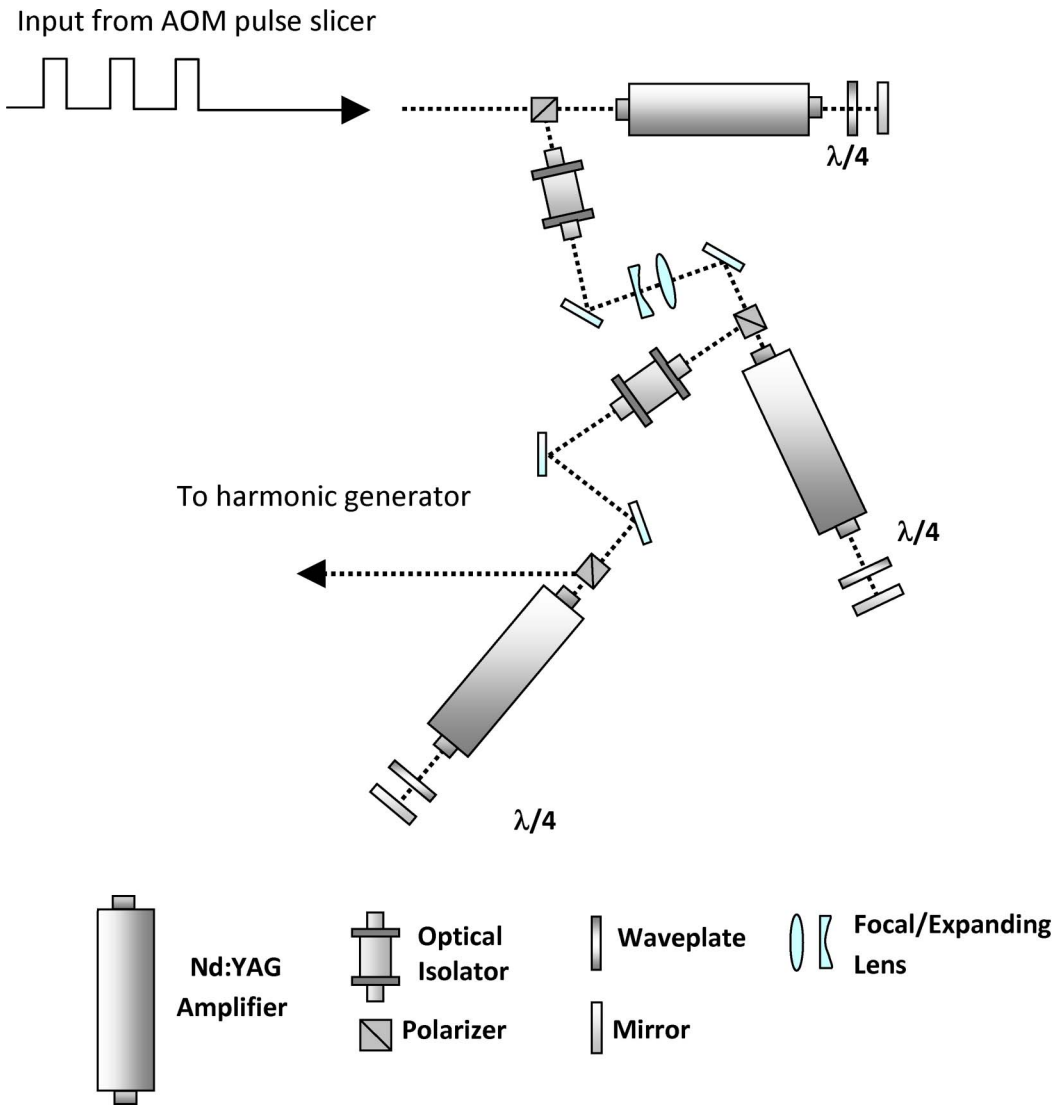

Fig. 3. (Color online) Schematic of power amplifier chain.

a width of approximately 200 μs. The energy within a pulse would thus depend on the delay between the flashlamp pulse and the Q switch. In the context of the pulse burst laser system, this results in a nonuniform distribution of energy among the burst of pulses. In the current design, the amplifiers were specified to have a nominally top-hat profile with a 1 ms long duration. This has two advantages. One, the distribution of energy among pulses within a burst will be more uniform; and, two, pulses can be created over a larger period of time, allowing for more flexible operation. For example, with a 1 ms window, the user can create a burst of 100 pulses at 100 kHz, whereas in previous designs the burst would have been limited to ~20 pulses at 100 kHz.

3. System Performance

System performance was assessed by using a combination of powermeter and photodiode measurements of the laser pulses after amplification. Figure 4 shows a burst of 68 pulses produced at a 500 kHz repetition rate. Each pulse is 40 ns long and the energy is approximately constant across the burst. For this burst, the power was approximately 130 mW, which corresponds to a peak power of 10 kW for each pulse

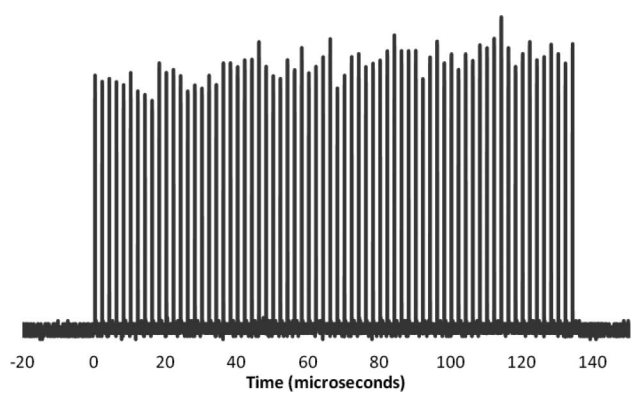

Fig. 4. Burst of 68 pulses at 500 kHz. Each pulse is 40 ns in duration.

and energy of ~0.4 mJ/pulse. Based on these measurements, the peak gain for the system is estimated to be approximately 2×10^5. The gain of individual amplifiers was measured to be approximately 100, 100, and 25 for the first, second, and third amplifiers, respectively, which agrees well with the measured overall gain of the system. In comparison with earlier-generation systems, these individual gain values are relatively low and can be increased by using a higher-power flashlamp controller.

Higher and lower repetition rates with a variable number of pulses and pulse durations were also examined and demonstrated similar characteristics to that shown in Fig. 4. For short pulses (<1 μs), it was found that the repetition rate and number of pulses did not significantly affect the peak power output of the individual pulses. The shape of the waveforms remained approximately the same (see Fig. 2) after amplification, with peak powers of over 10 kW achieved. The magnitude of the gain, however, does vary with the flashlamp delay time. The delay time is the time between the flashlamp pulse and the formation of the laser pulse. This behavior is shown in Fig. 5, which shows the relative gain versus delay time. There is an approximately 200 μs period before significant gain is available. Peak gain occurs for a delay of 700 μs, with the gain remaining within 10% of its peak value for a duration of ~500–600 μs. This is an improvement over earlier-generation systems, where the gain is available over only a ~100–200 μs window. It should be noted that the measurements for Fig. 5 were made by using a single 25 μs duration pulse to produce a signal above the noise floor (~2 mW) of the powermeter. The gain profile is slightly longer and more uniform for shorter-duration pulses.

The behavior of the system is slightly different for longer pulses (>1 μs) where saturation of the amplifiers plays a more prominent role. In the context of this work, saturation refers to the loss of gain experienced as energy is removed from the gain medium faster than it can be replenished by the flashlamps. This is depicted in Fig. 6, which shows the oscilloscope trace of a long-duration pulse. After ~1 μs, the power is seen to gradually decrease with time such

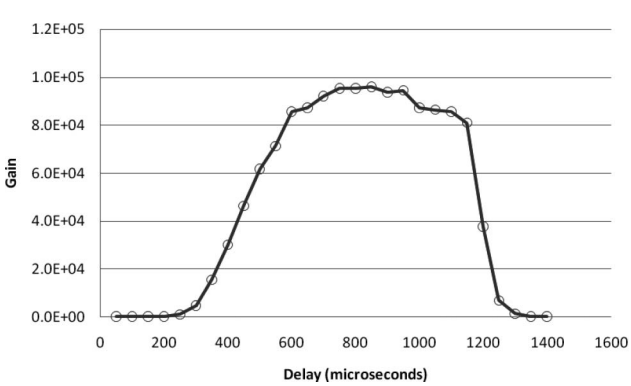

Fig. 5. Gain of power amplifier chain versus delay time for a 25 μs long input pulse.

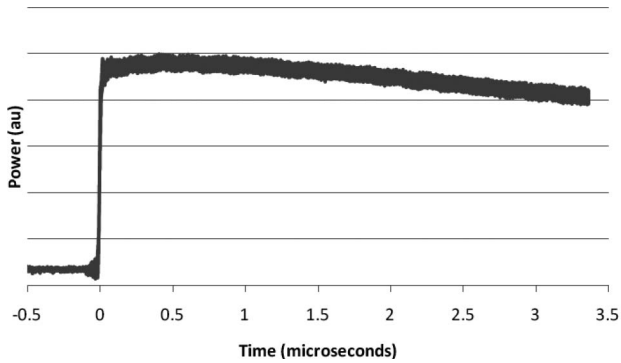

Fig. 6. Oscilloscope trace of long-duration pulse after amplification.

that the leading edge of the pulse experiences the largest gain. Thus, the leading edge of the pulse has the highest peak power (~10 kW), which gradually lowers with time. It is interesting to note that this drop is not evident with only two amplifiers running, indicating that saturation is not being reached until the third stage. This behavior is particularly important with respect to the pulse burst laser, as the first few pulses in a burst of pulses can act to remove energy from the system such that the gain is reduced for subsequent pulses. It is possible to counteract this energy depletion by beginning the formation of a burst of pulses earlier in the gain profile, where the gain is naturally lower. For example, uniform bursts of pulses with 350 ns long pulses were possible by setting the delay to ~450 μs. For 40 ns long pulses, such as shown in Fig. 4, the optimal delay was found to be ~540 μs. This is consistent with the idea that the longer pulse will deplete more energy from the system, necessitating a shorter delay. As more amplifiers are added to the system and the overall gain increases, we expect this to become an increasingly important issue. This problem can be partially avoided by utilizing larger Nd:YAG rods, which are capable of storing more energy, and using a single-pass gain configuration such that the first few pulses do not remove as much energy from the system. This strategy will be explored further in future work.

More details on the available energy for pulses can be found in Fig. 7, which shows the pulse energy versus pulse duration at an arbitrary delay time of 500 μs (see Fig. 5). Figure 7 shows the ability of the system to operate at pulse durations ranging from 20 ns to 50 μs with pulse energies in excess of 100 mJ/pulse realized at the longest pulse durations. The influence of saturation can be seen as the slope of the curve decreases with increasing pulse duration. In terms of power, the average power of a pulse decreases with increasing pulse duration. For a relatively long 50 μs pulse, the pulse energy is 120 mJ, which yields an average power of 2.4 kW over the duration of the pulse, which is less than the peak power. The peak power in this case is ~6 kW and occurs at the leading edge of the pulse as shown in Fig. 6. Nonetheless, the ability to easily change pulse duration provides the user with a tremendous

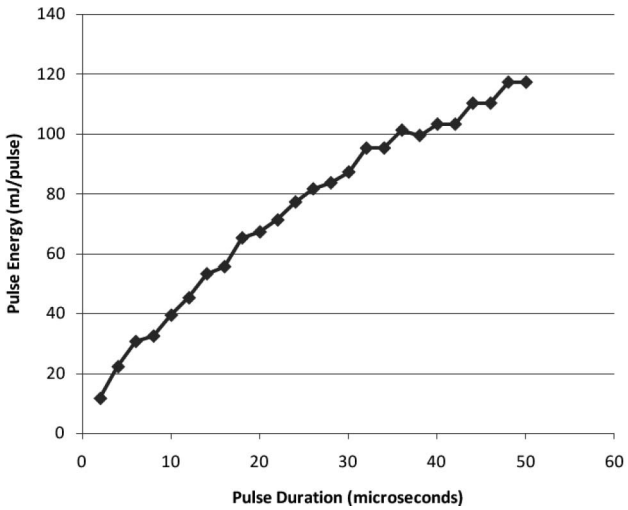

Fig. 7. Pulse energy versus pulse duration.

amount of flexibility in operating the system. For example, one limitation of Rayleigh scattering techniques is the optical breakdown in air due to the high intensity associated with a short-duration laser pulse. The current system would allow one to use a longer pulse and avoid this effect. Generally speaking, this capability is not available with conventional pulsed Nd:YAG laser systems.

An additional item worth noting is the presence of ASE, which can accelerate the effects of saturation by removing energy from the gain medium prior to amplification of the pulse train. ASE was measured to be approximately 4 mW with the amplifiers running but no laser pulses being fed into the power amplifier chain. Considering the long period of time over which gain is available, this is a negligible amount. As with the saturation effects, however, we expect this to become an increasingly important issue as more amplifiers are added to the system.

Last, second-harmonic generation was performed by directing the output through a type II KTP nonlinear crystal. Because of the relatively low intensity of the pulses at the ~6 mm exit of the final amplifier (~0.03 MW/cm^2), the beam was focused into the crystal by a 500 mm focal length plano-convex lens, forming an approximately 100 μm diameter spot, raising the average intensity to the order of 90 MW/cm^2. For a 150 ns duration pulse containing approximately 1.3 mJ of energy, conversion efficiencies as high as 35% were achieved by using this configuration. The conversion efficiency was reduced to ~10% by using a 1000 mm lens. Furthermore, the duration of the pulse did not have a noticeable effect on the conversion efficiency. One drawback to this arrangement is the increased potential for damage to the crystal due to our limited ability to control the intensity of the light. As such, we were unable to explore more efficient second-harmonic generation strategies. Still, these results demonstrate that the beam mode and contrast ratio are sufficient for efficient harmonic generation.

4. Conclusions and Future Work

The design of a third-generation megahertz-rate pulse burst laser system has been presented and demonstrated as suitable for the formation of high-energy, short-duration bursts of pulses at high repetition rates. In contrast to previous work, the pulse burst laser system presented here incorporates two key design improvements. The first is the use of an AOM for pulse slicing, and the second is the extension of the gain envelope to longer durations. Both changes were shown to be effective and to be improvements over earlier designs. The AOM is capable of producing pulses as short as 20 ns with a contrast ratio of the order of 20,000 : 1. In addition, the AOM is an order of magnitude less expensive than the Pockels cells used in earlier designs and provides more flexible operation owing to the 100 MHz bandwidth of the AOM driver. The extension of the gain envelope to longer pulse durations also adds additional flexibility to the formation of pulses, allowing a greater number of pulses to be formed at a given repetition rate. Overall, the system provides the user with a tremendous amount of flexibility as variable duration laser pulses can be formed on demand within the gain envelope of the system. This feature was demonstrated as pulses ranging from 20 ns to 50 μs were formed with pulse energies over 100 mJ/pulse. We hope to exploit this capability in future work to develop novel flow diagnostics not possible with conventional pulsed Nd:YAG laser systems.

One shortcoming of the current pulse burst laser system is the relatively low gain of the system. The gain of the current system is $\sim 2 \times 10^5$. This gain limited short-duration pulse energies to the order of 1 mJ/pulse and prevented further investigation into the effects of gain saturation and ASE, both of which are increasingly important for higher pulse energies. The gain achieved here is limited by the number of amplifier stages (three compared with five–six in earlier-generation systems) and the limited power available in the flashlamp power supply. Both of these issues will be resolved in the near future as we prepare to add two additional amplifiers and replace the flashlamp power supplies with more powerful units. Based on comparisons with similar laser systems, it is expected that these additions will increase the gain by nearly 2 orders of magnitude, allowing pulse energies of the order of 100 mJ/pulse over short bursts of pulses. We are particularly interested in exploring the effects of ASE and saturation at these high levels of gain, as these appear to be limiting factors in the expansion of the system to even higher powers and smaller form factors.

References

1. W. Koechner, *Solid-State Laser Engineering* (Springer, 1999).
2. B. S. Thurow, "Recent progress towards a high-speed three-dimensional flow visualization technique," in *22nd International Congress on Instrumentation in Aerospace Simulation Facilities, 2007. ICIASF 2007* (IEEE, 2007), pp. 1–7.
3. W. R. Lempert, P. Wu, B. Zhang, R. B. Miles, J. L. Lowrance, V. Mastracola, and W. F. Kosonocky, "Pulse-burst laser system

for high speed flow diagnostics," presented at the 34th AIAA Aerospace Sciences Meeting, Reno, Nevada, 15–18 Jan. 1996 (American Institute for Aeronautics and Astronautics), paper AIAA 96-0179.
4. P. Wu, W. R. Lempert, and R. B. Miles, "MHz pulse-burst laser system and visualization of shock-wave/boundary-layer interaction in a Mach 2.5 wind tunnel," AIAA J. **38**, 672–679 (2000).
5. B. Thurow, N. Jiang, M. Samimy, and W. Lempert, "Narrow-linewidth megahertz-rate pulse-burst laser for high-speed flow diagnostics," Appl. Opt. **43**, 5064–5073 (2004).
6. B. Thurow, N. Jiang, W. Lempert, and M. Samimy, "MHz rate planar Doppler velocimetry in supersonic jets," AIAA J. **43**, 500–511 (2005).
7. M. Wernet and A. Opalski, Development and application of a MHz frame rate digital particle image velocimetry system, presented at 24th AIAA Aerodynamic Measurement Technology and Ground Testing Conference, Portland, Oregon, 28 June to 1 July 2004 (American Institute for Aeronautics and Astronautics), paper AIAA-2004-2184.
8. A. Kastengren, J. C. Dutton, and G. Elliott, "Time-correlated visualizations of supersonic blunt-base cylinder wakes," presented at 43rd AIAA Aerospace Sciences Meeting and Exhibit, Reno, Nevada, 10–13 Jan. 2005 (American Institute for Aeronautics and Astronautics), paper AIAA-2005-1346.
9. A. Korpel, *Acousto-Optics* (Marcel Dekker, 1996).